Advances in Geosciences
Vol. 18: Ocean Science (2008)
Eds. Jianping Gan *et al.*

TROPICAL PACIFIC UPPER OCEAN HEAT CONTENT VARIATIONS AND ENSO PREDICTABILITY DURING THE PERIOD FROM 1881–2000

YOUMIN TANG* and ZIWANG DENG
Environmental Science and Engineering
University of Northern British Columbia,
Prince George, BC, Canada
**ytang@unbc.ca*

In this study, a long-term analysis of the tropical Pacific upper ocean heat content (HC) was obtained for the period from 1881–2000, by assimilating historic sea surface temperature dataset into an oceanic general circulation model (OGCM) with Ensemble Kalman filter. The validation against the NCEP (National Center of Environmental Prediction) HC and the observed HC indicates that the analyzed HC captures very well the large-scale observed features of HC. There exists a striking interannual variability in the tropical Pacific upper ocean HC anomalies (HCA). Like ENSO (El Niño and the Southern Oscillation), the HCA interannual variability also has a significant interdecadal variation. The interdecadal variation in the HCA causes the interdecadal variation in the lagged correlation between the HCA of the equatorial western Pacific ocean and the SSTA (sea surface temperature anomalies) of the equatorial eastern Pacific, which in turn affects ENSO prediction skill (Niño3.4 SSTA). The long-term retrospective ENSO prediction from 1881–2000 by the model supported the above conclusion.

1. Introduction

The tropical Pacific upper hear content (HC) is an important component of the coupled ocean-atmosphere system of the tropical Pacific ocean on the interannual timescale, and a major source of memory for the system. It plays an essential role in the oscillation of the ENSO cycle by controlling the temperature of the waters upwelled in the eastern equatorial Pacific. The link of ENSO variability to the heat content build-up and discharge in the tropical Pacific has been evidenced in theory and observation (e.g. Wyrtki, 1985; Suarez and Schopf, 1988; Battisti, 1988; Jin, 1997). It has been found that the HC redistribution in the western tropical Pacific can

lead to the evolution of SST anomalies in the eastern Pacific and has been known to be an important factor in the evolution of many ENSO episodes. In particular, the HC anomalies over the equatorial band 5°N to 5°S can be a very good precursor for the SST anomalies in the Niño3 region (5°N–5°S, 150°W–90°W) (e.g. Zebiak, 1989; Latif and Graham *et al.*, 1992; Meinen and McPhaden, 2000; Kessler, 2002; Trenberth *et al.*, 2002; McPhaden, 2003; Yu and Kao, 2007). The equatorial Pacific HC also is a useful predictor of Indian summer monsoon rainfall (Rajeevan and McPhaden, 2004).

There is a large body of literature studying the HC variability and its link to ENSO in the past decades (e.g. review papers by Latif *et al.*, 1998 and Neelin *et al.*, 1998; McPhaden, 2003; White, 1995; Lohmann and Latif, 2005). However all of these studies only cover time periods of 20–50 years due to a lack of long-term subsurface observations. The period available for studying HC variability at interannual time scale, in particular at the decadal time scale, probably precludes statistically robust conclusions. Therefore it is of interest and practical importance to explore the possibility to obtain long-term HC data, thereby effectively studying HC variability. An effective method towards this goal is to generate a long-term analysis dataset of HC using the state-of-the-art models and using other long-term observations available. With the development of assimilation technique in recent years, the reanalysis strategy has accepted intensive attention. In fact, the reanalysis NCEP and ECMWF wind datasets have been widely used as the "observations" since they were generated.

This study attempts to produce a long-term HC analysis dataset over 100 years through an OGCM, and then to further explore the variability of the upper oceanic heat content. Recently we reconstructed the surface wind stress of the tropical Pacific for the period from 1875–1947 using statistical technique and using the historic SST and sea level pressure datasets (Deng and Tang, 2008), which enables it available to implement a long-term control run of the OGCM. The reconstructed wind stress has been successfully applied to perform retrospective ENSO prediction for the past 120 years (Deng and Tang, 2008; Tang *et al.*, 2008), suggesting the high quality and good credits of the reconstructed wind. Further, we recently also completed the assimilation of a long-term historic SST dataset into the OGCM that led to skillful retrospective predictions (Deng *et al.*, 2008). All of these allow us to produce a long-term analysis of the upper ocean heat content for the tropical Pacific.

This paper is structured as follows: Section 2 briefly describes the model, data and assimilation scheme. Section 3 examines the quality of

analyzed HC by comparing it against the NCEP reanalysis dataset for their common period from 1980–2000, as well against the observed HC from 1961–2000. In Secs. 4 and 5, the HC variability and its link to ENSO are investigated for the period from 1881–2000. A summary and discussion are given in Sec. 6.

2. Model, Data and Assimilation Scheme

2.1. *Data*

In this study we used the monthly Extended Reconstruction version2 SST (ERSST.v2) dataset from 1878–2002, reconstructed by Smith and Reynolds (2004), with a resolution of $2^\circ \times 2^\circ$. The data domain was configured for the tropical Pacific ocean. This bias corrected dataset has been used for studying climate variation and prediction (e.g. Xue *et al.*, 2003; Nakaegawa *et al.*, 2004; Monahan and Dai, 2004). Due to relatively poor quality of the dataset prior to 1881, we focus on the period from 1881–2001 in this study. For the validation of SST assimilation, the NCEP reanalysis subsurface temperature from 1980–2000 is also used in this study (Behringer *et al.*, 1998; referred to as the NCEP data hereafter). The data domain is confined in the tropical Pacific Ocean, spanning from 1980 to 2000 with the resolution of 1.0° lat. by 1.5° lon.

The monthly 400 m depth-averaged heat storage anomalies from the Joint Environmental Data Analysis Center at the Scripps Institution of Oceanography. This data set consists of all available XBT, CTD, MBT and hydrographic observations, optimally interpolated by White (1995) to a three-dimensional grid of 2° lat. by 5° lon., and 11 standard depth levels between the surface and 400 m. This dataset is referred to as the observation although it is still, strictly saying, a kind of reanalysis dataset.

To perform a long-term analysis with an OGCM, the past wind stress data, as the model forcing, is required. Using SST as a predictor and SVD technique, a long-term wind stress dataset from 1881–1947 was reconstructed, with the resolution $2^\circ \times 2^\circ$ and the domain of tropical Pacific from 30°S–30°N (see http://web.unbc.ca/ytang/wind.html). The cross-validation scheme was used in the reconstruction to ensure the training data not used in test periods. The training data of the wind is the NCEP reanalysis 10 m wind speed in monthly T62 Gaussian grids for 1948–2006 (Kalnay *et al.*, 1996). For consistency, we also used the reconstructed surface wind for the period from 1948–2001 instead of the observed wind

in this study. The reconstructed wind has been applied to study ENSO predictability as mentioned in the introduction.

HC is defined here as the integral of the temperatures over the first 17 model levels, equivalent to the depth of 250 m, calculated from

$$HC = \frac{\sum_{i=1}^{17} h_i T_i}{\sum_{i=1}^{17} h(i)}, \tag{1}$$

where T_i and h_i are the temperature and depth of level i.

2.2. *Model*

The ocean model used in this study is the latest version of NEMO (Nucleus for European Modeling of the Ocean), identical to that used in Tang *et al.* (2008) and Deng and Tang, (2008). Details of the ocean model are described in http://www.lodyc.jussieu.fr/NEMO/. The domain of the model used here is configured for the tropical Pacific Ocean from 30°N–30°S and 122°E–70°W, with horizontal resolution 2.0° in the zonal direction and 0.5° within 5° of the equator, smoothly increasing to 2.0° at 30°N and 30°S in the meridional direction. There are 31 vertical levels with 17 concentrated in the top 250 m of the ocean. The time step of integration is 1.5 hours and all boundaries are closed, with no-slip conditions.

The model was first spun up for 500 years using climatological wind stress derived from the 50-year NCEP Reanalysis wind stress and the heat flux Q_s is parametrized by model temperature as follows:

$$Q_s = Q_0 + \lambda(T - T_0), \tag{2}$$

where Q_0 is the climatological heat flux, obtained from the European Center for Medium-Range Weather Forecasts (ECMWF) reanalysis project for the base period 1971–2000. T is the model SST, T_0 is Levitus observed climatological SST (Levitus 1998), and λ is the relaxation rate, set to $-40\,\mathrm{Wm^2\,K^{-1}}$ (Tang *et al.*, 2004; Moore *et al.*, 2006). For a 50 m mixed-layer depth, this value corresponds to a relaxation time scale of two months (Madec *et al.*, 1998).

2.3. *Assimilation scheme*

The ERSST.v2 data from 1881–2000 was assimilated into the OGCM using Ensemble Kalman Filter (EnKF). The assimilation domain covers

the tropical Pacific from 140°E to 80°W and 15°S to 15°N in horizontal and in the upper 17 levels (250 m). The assimilation was performed by every 5 days.

Usually SST is a prognostic variable in ocean models, and the general procedure of SST assimilation is to optimally insert it into the models. However this strategy is unable to effectively correct the subsurface temperature, leading to serious imbalances between the surface and subsurface during the assimilation cycle (Tang and Kleeman, 2002). Therefore, a key issue for SST assimilation is an effective vertical transfer of information from the surface to the subsurface. Towards this goal, a special strategy of initial perturbation is used in this study to generate ensemble, namely that the perturbation field is designed to be of not only horizontal coherence but vertical coherence between adjacent levels. The vertical coherence is considered using the below method

$$\epsilon_k = \alpha\epsilon_{k-1} + \sqrt{1-\alpha^2}W_k, \tag{3}$$

where ϵ_k is the pseudorandom field at the kth level ($k = 1, 2, \ldots, 17$), and W_k is the pseudorandom field at the kth level without considering vertical coherence, constructed using the method of Evensen (2003).

With such a well-designed perturbation scheme, the forecast error covariance matrix in EnKF can act as a time-variant transfer operator to project the SST corrections onto the subsurface temperatures effectively (Deng *et al.*, 2008). As such the increments of subsurface temperatures can be obtained via the transfer operator during assimilation cycles. The details of the assimilation system by EnKF can be found in Deng *et al.* (2008).

3. Validation of the HC Analysis from 1980–2000

A long-term control run was performed with the OGCM, forced by the reconstructed wind from 1881–2000. In this control run, the SST was also assimilated into the OGCM sequentially every five days from 1881–2000 using EnKF with a well-designed perturbation scheme as aforementioned. From the long-term assimilation run, we obtained a long term analysis for all variables of the OGCM including SST and subsurface temperatures. The SST analysis and the retrospective ENSO predictions initialized from these analyses were discussed in details in Deng *et al.* (2008). In this section, we will validate HC analysis through comparing it with the NCEP HC dataset of the upper 250 m that assimilated both altermetry data and observed

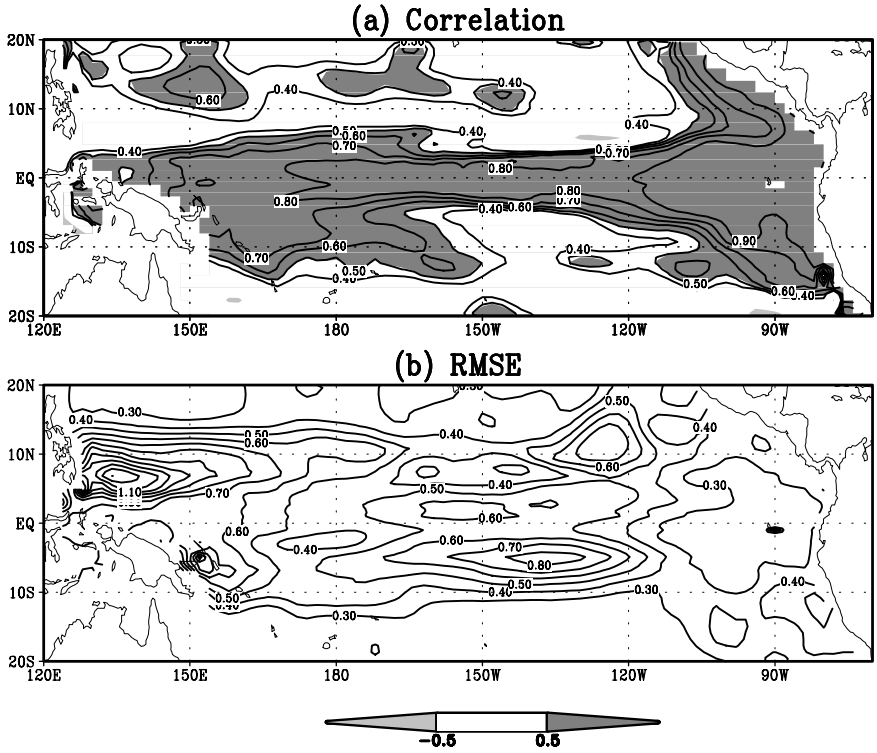

Fig. 1. (a) Anomaly correlation R and (b) $RMSE$ between the analyzed HC and the NCEP HC for the period from 1980–2000.

SST, and with the monthly 400 m depth-averaged heat storage anomalies from Scrippts Institution that consists of all available XBT, CTD, MBT and hydrographic observations.

Figure 1 shows the correlation and RMSE (root mean square error) between the analyzed HCA and the NCEP counterpart for the period from 1980–2000. The best analysis skill appears in the eastern Pacific and the whole equatorial belt, with correlation coefficient over 0.7. The HC analysis is relatively poorer in the region 10° off the equator. This is due mainly to two reasons: (i) the assimilation domain is confined within the equatorial belt of 15° based on the consideration of computation expense; (ii) the OGCM only has good simulation skills in the equatorial belt. The poor simulated skills off the equator are common defects in almost all ocean models including OGCMs (e.g. Deng *et al.*, 2008; Lou *et al.*, 2005). The good HC analysis in the equatorial Pacific is important and has practical

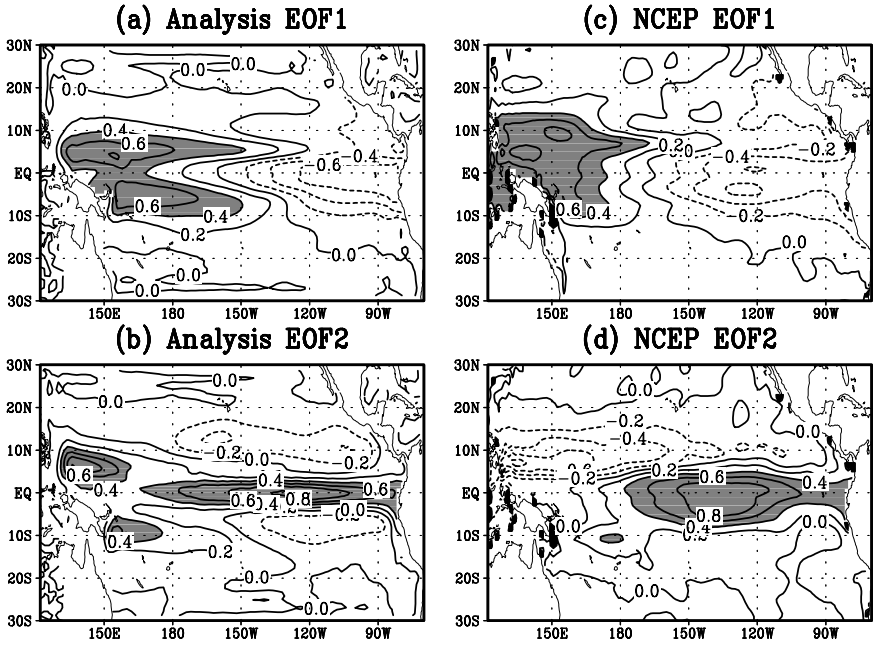

Fig. 2. The first and second EOF modes for the analyzed HC (a and b) and the NCEP HC (c and d).

significance since the strongest coupling of the air-sea occurs there, and the HCA distribution along the equator dominates ENSO characteristics and evolution.

Figure 2 compares two leading EOF modes of the analyzed HCA with those derived from the NCEP HCA during 1980–2000. The two EOFs of the analyzed HCA account for 78% and 14% of the total variance, respectively, which compare with 33% and 15% of the total variance accounted for by two leading modes from the NCEP HCA. The larger variance accounted for by the leading modes of the analyzed HCA is probably because the reconstructed wind stress that removed the high frequent components forced the ocean model. As seen in Fig. 2, the leading EOFs for the analyzed HCA (Figs. 2(a) and 2(b)) generally resembled the NCEP modes (Figs. 2(c) and 2(d)), except a stronger zonal HCA gradient at the equatorial central Pacific. The major characteristics of the first mode (Figs. 2(a) and 2(c)) has a dipole zonal structure involving a western Pacific "Rossby wave-like" response of one sign and an eastern Pacific "Kelvin wave-like" response of the opposite sign; whereas the second mode (Figs. 2(b) and 2(d)) has

a large-amplitude signal of the one sign located mainly in the equatorial central/eastern Pacific. These patterns agree with the idea of a heat content buildup prior to El Niño as postulated by Wyrtki (1985) and Jin (1997), and are consistent with the delayed-action oscillator mechanism (e.g. Battisti, 1988; Suarez and Schopf, 1988). They are also very similar to those reported in previous work (e.g. Tang *et al.*, 2005). Comparing leading modes between the analyzed HCA and the NCEP HCA reveals that the former has a stronger zonal HCA gradient at the equatorial central Pacific and a more obvious wave-like structure along the equator, probably because it was derived from the OGCM forced with the high-frequency free reconstructed wind stress.

Comparison of the leading principal components (PCs) between the analyzed and NCEP HCA is shown in Fig. 3. As can be seen, the analyzed HCA PCs are in very good agreement with the PCs of NCEP HCA, with their correlation coefficients over 0.8. This is also true for the averaged HCA over several Niño regions as shown in Fig. 4. However the analyzed HCA

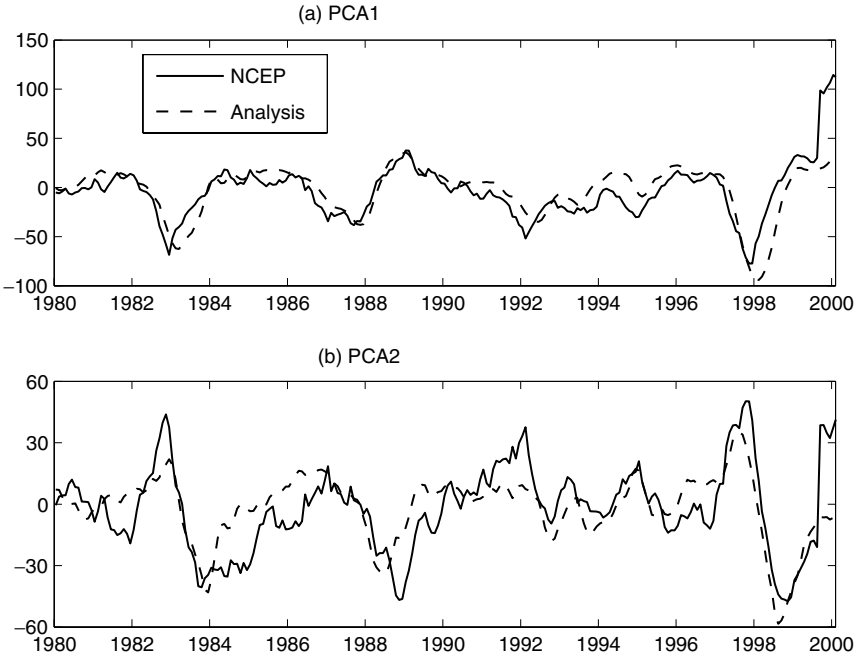

Fig. 3. Variations of the first and second principal components for the analyzed and the NCEP HC.

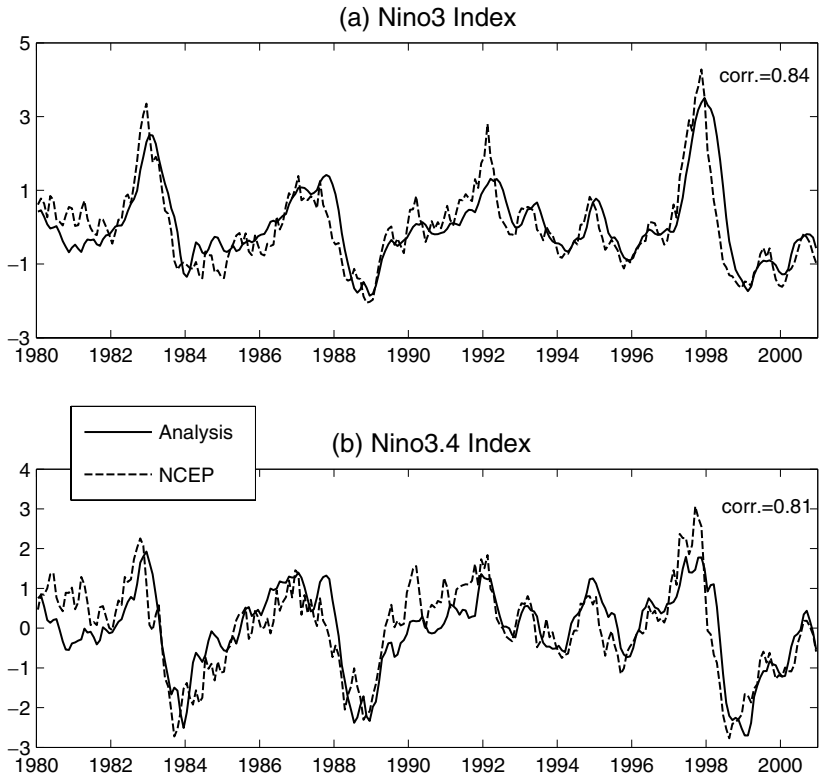

Fig. 4. Variations of the analyzed and the NCEP HC anomalies, averaged over the (a) Niño3 and (b) Niño3.4, for the period from 1980–2000.

leads NCEP HCA by 1–2 months, which may be due to the model bias in the OGCM. It was found that the model bias often results in the simulation of temperature anomaly variation leading the observation by 1–2 months in many oceanic models (e.g. Tang *et al.*, 2001).

Figure 5 shows the time-longitude plot of HCA along the equator during 1980–2000, taken from the analyzed and the NCEP data. As shown in Fig. 5, the analyzed HCA agreed well with the NCEP HCA, and captured all observed ENSO signals. The common deficiency for the analysis is relatively weak simulated amplitude, which is a common problem in many OGCMs.

We repeated all validations performed above using the observed heat storage (HS) of the upper 400 m for 1961–2000. The results are similar to those shown above. For example, Fig. 6 shows the correlation coefficients between the analyzed HCA against the observed HS anomalies, which is

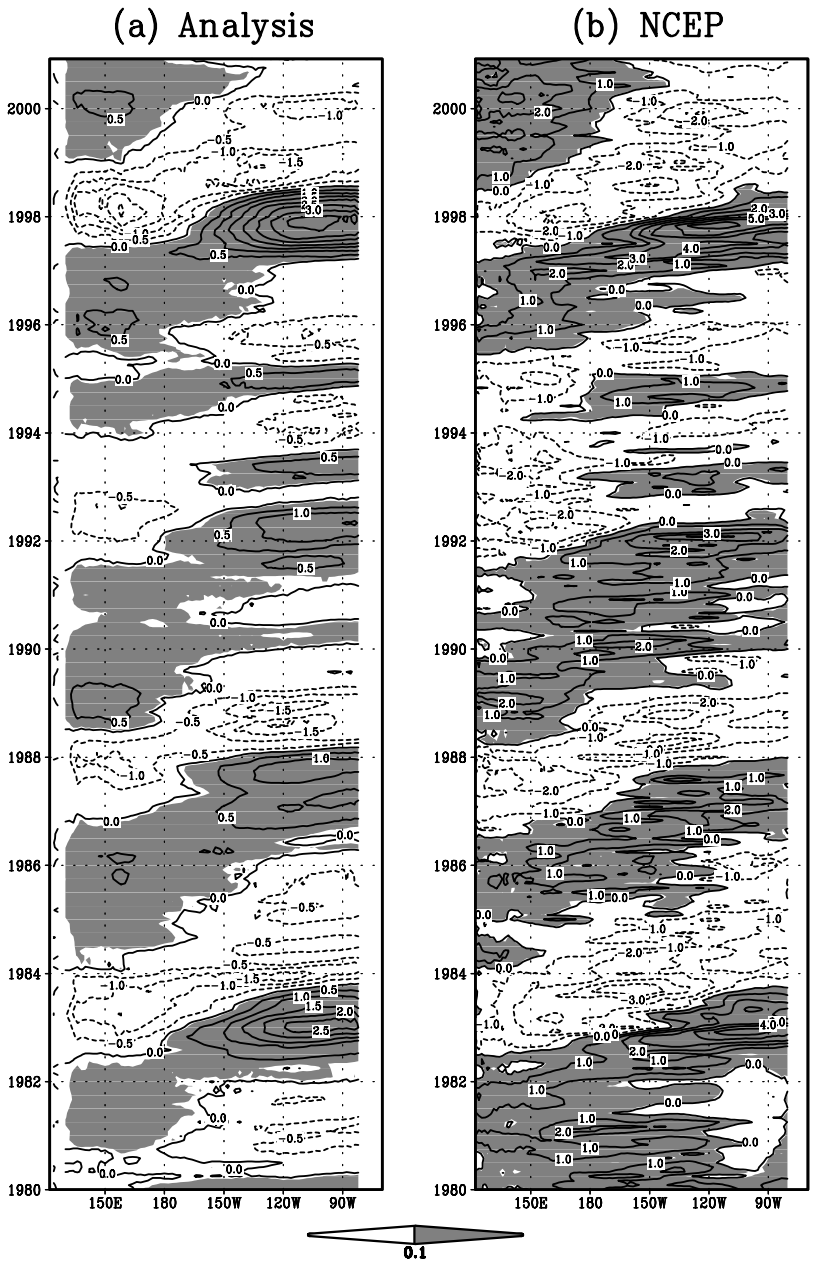

Fig. 5. Time-longitude diagrams along the equator, from (a) the analyzed HC and (b) the NCEP HC. Contour interval is 0.5° C in (a) and 1.0° C in (b). The positive anomalies above 0.1° C are shaded.

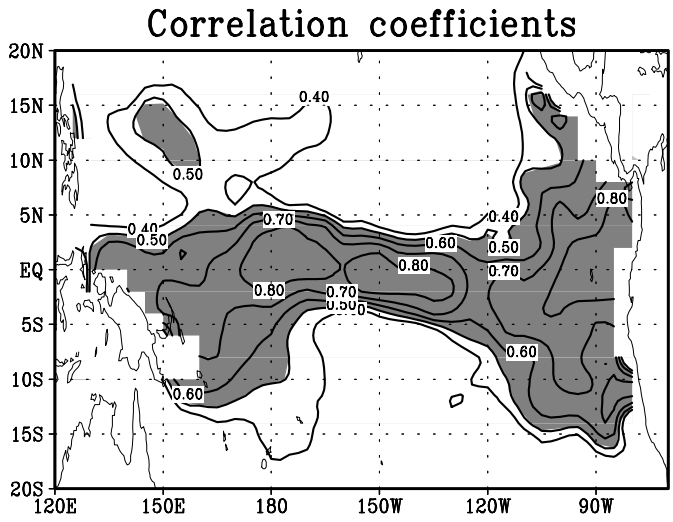

Fig. 6. Correlation between the analyzed HC and the observed HC for the period from 1961–2000.

very similar to Fig. 1(a). It should be noticed that HS data is defined as the integral of temperature over the depth multiplied by a constant coefficient and has a different unit (Watt-Seconds/Meter^2) from the analyzed and the NCEP HC, thus it is meaningless to compare their amplitude.

In summary, the analyzed HC can well characterize the realistic variations of the upper oceanic heat at monthly or longer time scales. It allows us to explore the upper ocean thermal states, in particular the HC variability at the interannual or longer time scales.

4. Variability of HC from 1881–2000

Figure 7 shows the evolution of the analyzed HCA along the equator from 1881–2000. The most striking feature in this time-longitude diagram is the interannual variability of HCA with a period of 2–5 years during the whole period. Comparing the interannual variability of HCA with ENSO variability of SSTA (not shown) reveals a very good relationship between them, namely that, the analyzed HCA captures well all ENSO events from 1881–2000. A further scrutiny of Fig. 7 finds that the interannual variability of HCA has decadal/interdecadal variation as in that of SSTA (Tang *et al.*, 2008). For example, the magnitude of HCA is visibly larger during the period from 1980–2000 than during other periods whereas the

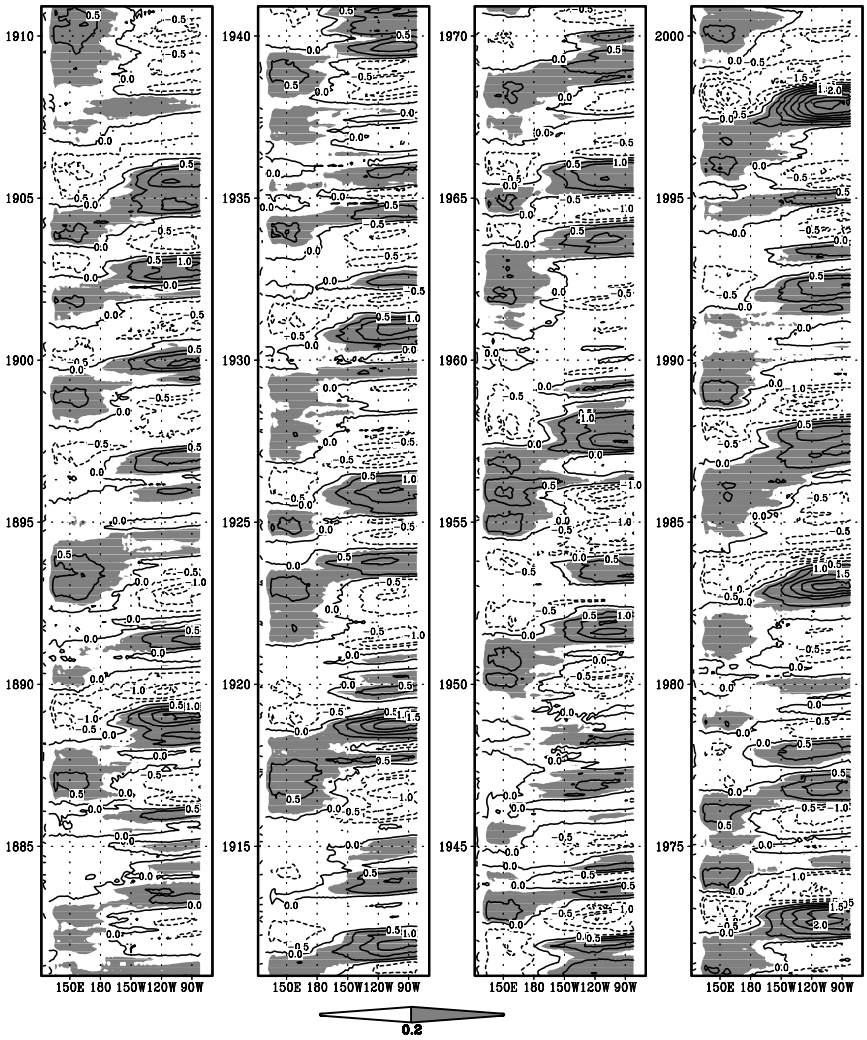

Fig. 7. Same as Fig. 5 but for the period from 1881–2000.

HCA is likely to have the smallest magnitude in the 1920s and 1930s. Such a decadal/interdecadal variation in HCA interannual variability is more obvious in Fig. 8, which shows the wavelet power spectrums of the first two principal components of HCA. The local wavelet power spectrum clearly indicates that the significant periods are localized in time. During 1960–2000, the signal is significant at the periods of 2–5 years whereas

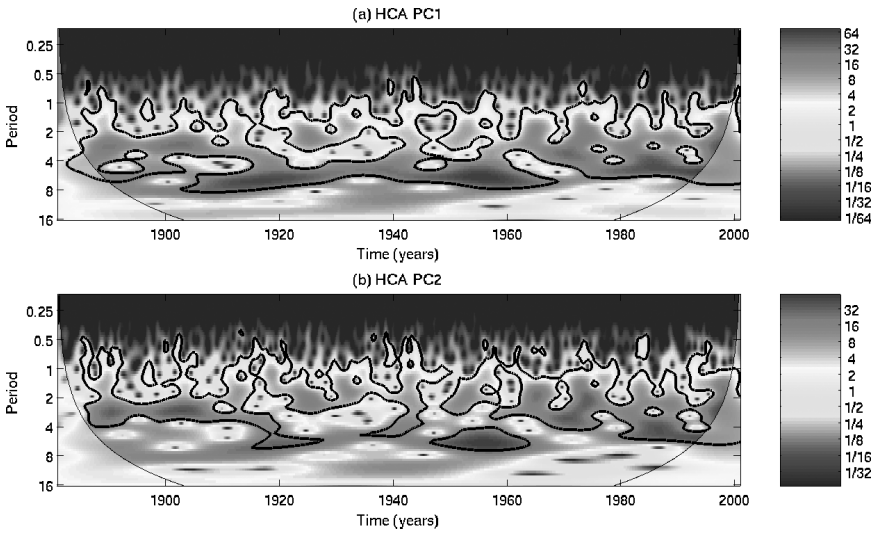

Fig. 8. The wavelet power spectrum of (a) HCA PC1 and (b) HCA PC2. The power spectrum is normalized by 95% confidence critical power calculated by Monte Carlo significant test method. The area under the arc line is the cone of influence, where zero padding has reduced the variance. Black contour is the 5% significance level, using a red-noise (autoregressive lag 1) background spectrum. The period of unit (y-axis) is year.

during 1905–1960 the strong signal appears at the periods of 4–8 year with weak signal at the periods of 2–4 years. One might speculate that the interdecadal variation of HCA interannual variability is due probably to the data quality since the observations were very sparse and sporadic, even unavailable before 1960. However, there were strong ENSO signals at the periods 2–5 years before 1905, which might effectively remove such a speculation.

The interdecadal variations in HCA interannual variability are further displayed in Fig. 9, which shows the variation of the strength of ENSO signal measured in each running window of 20-yr from 1881–2000 (i.e. 1881–1900, 1882–1901, . . ., 1981–2000).[1] For comparison, the ENSO signal of SSTA is also presented. Two methods were applied to extract the ENSO signal in this study. The first was to perform spectrum analysis for the first principal component (PC1) of the analyzed HCA and observed SSTA, respectively,

[1]The signal measured during a 20-yr window is plotted at the middle point of the window in Fig. 9. For example, the signal at 1890 was calculated using the samples from 1881–1900. The 20-yr window is shifted by one year each time starting from 1881 until 2000.

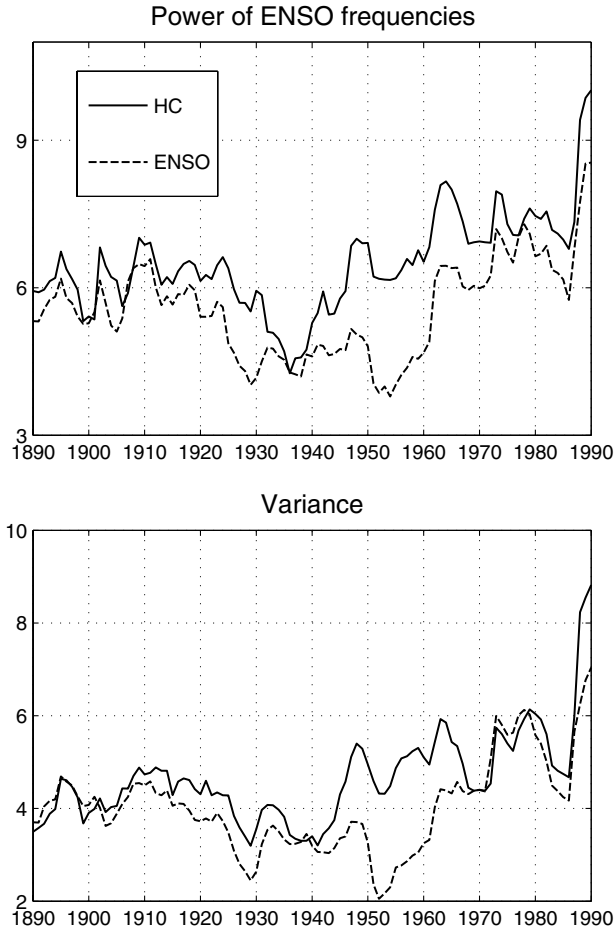

Fig. 9. The strength of the interannual variability of SSTA and HCA, measured by (a) the spectrum power at ENSO frequencies of 2–5 years of PC1 and (b) the variance of PC1, both calculated in each 20-yr running window from 1881–2000.

for each 20-yr running window, using the total spectrum power at the frequencies of 2–5 years to represent the strength of ENSO signal, as shown in Fig. 9(a). The second was to use the variance of the analyzed HCA PC1 and observed SSTA PC1, computed for each running window of 20-yr from 1881–2000, as shown in Fig. 9(b). The two methods produce very consistent results. Figure 9 shows a significant interdecadal variation in ENSO signal in both the surface temperature and the subsurface heat content, and a consistent relationship between the variation in SSTA and that in HCA.

In the late 19th century and the early 20th century, ENSO signal was relatively strong and stable. Since the early 1920s, the signal strength was weakened, reaching a minimum around 1940s, beyond which the signal rebounded and increased with time until the 1960s. ENSO signal was the strongest from the 1960s, especially in the late 20th century. Therefore, there is a striking interdecadal variation of ENSO signal in the upper heat content anomalies of the tropical Pacific during the past 120 years from 1881–2000. In the next section, we will see the interdecadal variation of ENSO signal is a major reason to cause the interdecadal variation in ENSO prediction skill.

5. HC Variability and ENSO Predictability

It has been reported in several recent works that ENSO predictability has decadal/interdecadal variation, which was argued to be due mainly to the corresponding decadal/interdecadal variation in ENSO variability (e.g. Chen *et al.*, 2004; Tang *et al.*, 2008; Deng and Tang, 2008). In this section, we will examine the relationship of decadal/interdecadal variations between ENSO predictability and HCA variability, which has been so far little addressed. Towards this goal, a long-term retrospective ENSO prediction was performed for the period from 1881–2000 using the hybrid coupled model (HCM), i.e. the OGCM coupled with a statistical atmospheric model. The statistical atmospheric model is a linear model that predicts the contemporaneous surface wind stress anomalies from SSTA, which was constructed by the singular vector decomposition (SVD) method with cross-validation scheme. During the initialization of the hybrid coupled model, the OGCM was forced by the sum of the associated wind anomalies computed from the atmospheric model and the observed monthly mean climatological wind stress. Full details of the HCM are given in Deng *et al.* (2008) and Tang *et al.* (2004, 2008).

A total of 480 forecasts, initialized from January 1881 to October 2000, were run starting at three months intervals (1 January, 1 April, 1 July, 1 October), and continued for 12 months for the HCM. The SST assimilation was performed to initialize the forecasts as introduced in Sec. 2.3.

Figure 10 shows the averaged correlation R and MSE (mean square error) over 1–12 months lead measured in each running window of 20-yr from 1881–2000 (thin blue line and dashed green line), i.e. 1881–1900, ..., 1981–2000, where the predicted Niño3.4 SSTA (5°N–5°S,

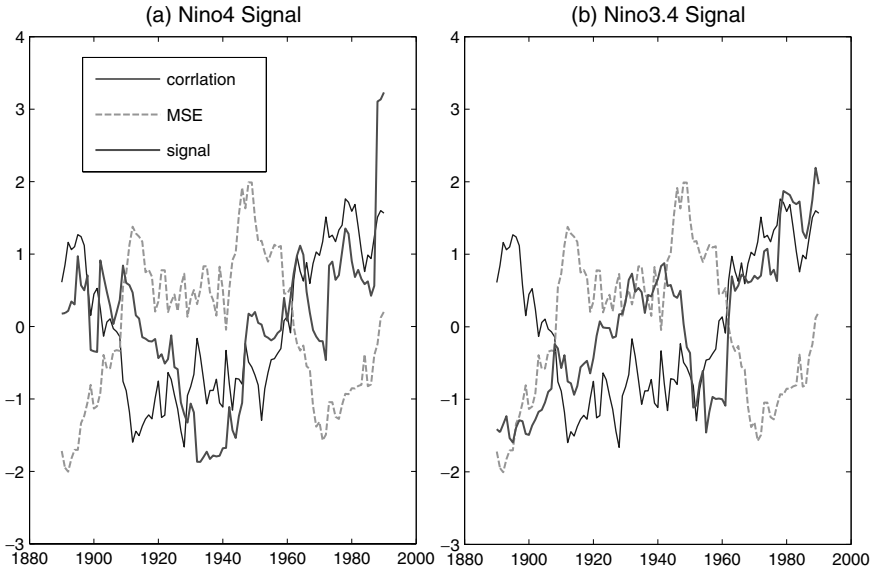

Fig. 10. The averaged prediction skill of Niño3.4 SSTA index over the first 12 month leads, against the HC signal measured by (a) HCA Niño4 index and (b) HCA Niño3.4 index. The evaluation was done in each 20-yr running window from 1881–2000. The normalization was applied prior to plotting for removing the unit.

170°W–120°W) is compared against the observed value. As can be seen, there is a striking interdecadal variation of ENSO predictability in the past 120 years from 1881–2000 in the HCM. Generally there is a high predictability in the late 19th century and in the middle-late 20th century, and a low predictability from 1901–1960. Figure 10 also displays the signal of HCA in Niño4 (5°N–5°S, 160°E–150°W) (Fig. 10(a)) and in Niño3.4 (Fig. 10(b)) (thick red line), respectively, measured by their individual variance.

Figure 10(a) demonstrates a significant relationship between the ENSO predictability and the signal of Niño4 HCA. Both display a consistent interdecadal variation. In the late 19th century, the signal was strong, and the model showed a large correlation R and a low MSE. Since then the signal strength weakened and the skill continuously declined with time, both reaching a minimum around 1940s, beyond which both rebounded and increased with time until the 1960s. The model has a relatively good prediction skill from the 1960s, especially in the late 20th century. Correspondingly, the Niño4 HCA signal is also the strongest

in these periods. Such a good relationship between Niño4 HCA signal and prediction skills holds not only for correlation R but also for *MSE* skill.

Figure 10(b) shows the Niño3.4 HCA signal (thick red line), which is somehow different from that of Niño4. For example, the Niño3.4 HCA signal was week in the late 19th century but relatively strong during the period from 1901–1940, which was almost out of the phase of that of Niño4. The overall relationship between Niño3.4 HCA signal and ENSO predictability is weak in Fig. 10(b), although there is a good relationship after the late 1960s. This is different from the relationship between Niño3.4 SSTA signal and ENSO predictability, which is significantly strong for the whole period (Tang *et al.*, 2008). We also explored the relationship between ENSO predictability and the HCA signal measured using PC1 and Nino3 index, respectively, and got similar results.

It is of interest to explore the underlying physical interpretation of the relationship between Niño4 HCA signal and prediction skill. As discussed in the introduction, the most important physical and dynamical process responsible for ENSO cycle probably is the "Discharge" mechanism of the upper HC of the equatorial western Pacific or "Delayed oscillator mechanism", both asking a significant lagged relationship between the Niño4 HCA signal and the Niño3 (Niño3.4) SSTA signal. Indeed, it has been found in many ENSO prediction models that the model predication skill is usually high when the lagged correlation is strong, and the Niño4 HCA is a very good precursor of Nino3 (3.4) SSTA evolution (e.g. Latif *et al.*, 1998; Tang and Hsieh, 2003).

Shown in Fig. 11(b) is Niño3.4 SSTA prediction skill measured in 6 sub-periods of 20 years each. It is evident in Fig. 11(b) that the correlation skills are significantly different among these periods. Comparing Figs. 10 and 11(b) reveal a considerable consistency of variations in correlation skill. For example, high prediction skills appear in the late 19th century and the middle-late 20th century, i.e. 1881–1900, 1961–1980 and 1981–2000, whereas the periods of 1901–1920, 1921–1940, and 1941–1960 have relatively low prediction skills. A similar consistency is also found in the *MSE* skill (not shown). Figure 11(a) shows the lagged correlation between the analyzed Niño4 HCA and the observed Niño3 SSTA, with SSTA leading to HCA. As can be seen, the period that has a high prediction skill has also a good lagged correlation and vice versa. For example, the best correlation prediction skills appear in the middle-late 20th century when the lagged correlation is the highest during this period whereas the periods that have

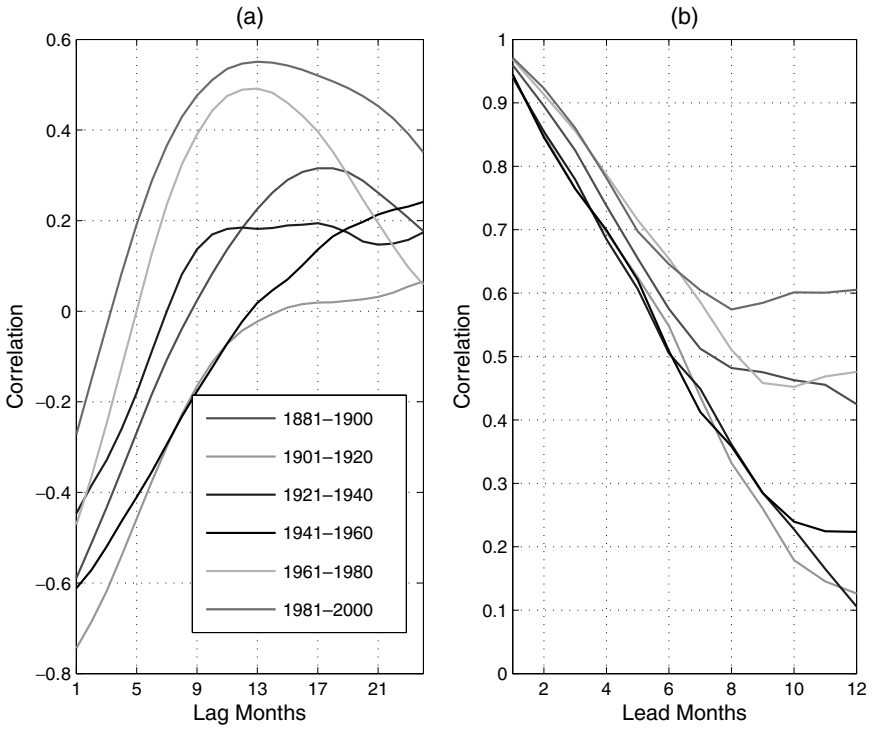

Fig. 11. (a) The lagged correlation between Niño4 HCA index and Niño3 SSTA index, with the HCA behind SSTA, for six different periods; (b) the correlation skill between predicted Niño3.4 SSTA index against the observed value, as a function of leading time, for the corresponding periods.

the minimum lagged correlation have very poor skills such as 1941–1960 and 1901–1921.

In summary, there is a striking interdecadal variation of ENSO predictability in the past 120 years from 1881–2000, which is highly related to interdecadal variation of the signal of Niño4 HCA. When the signal of Niño4 HCA is stronger, the lagged correlation between it and the equatorial eastern Pacific SSTA is larger, leading to better prediction skills.

6. Discussion and Summary

An important step in understanding ENSO and the interaction of air-sea of the tropical Pacific ocean is to analyze the upper ocean heat content, as evidenced in a large body of literature. However all studies about the

tropical pacific upper ocean HC have been so far confined within the last 20–50 years due to the unavailability of the longer data, which is not long enough to study HC variability at the interannual and decadal scales.

In this study, we explored the possibility of producing a long-term HC analysis dataset over 100 years through an OGCM and a well-designed EnKF-based assimilation system for the historic SST dataset. The results show that the analyzed HC, compared with the NCEP data and the observation, well characterizes the realistic variability of the HC at monthly or longer time scales. The correlation coefficients between the analyzed HC with the NCEP HC are very high up to 0.9 in the equatorial eastern Pacific ocean. It is also true when the analyzed HC is validated against the observed HC.

Further we examined the variation of the tropical Pacific upper ocean HC from 1881–2000. It was found that there exists a striking interannual variability in the tropical Pacific upper ocean HCA. Like ENSO variability, the HCA interannual variability has also a significant interdecadal variation. In the late 19th century and the early 20th century, the HC interannual signal was relatively strong and stable. Since the early 1920s, the signal strength was weakened, reaching a minimum around 1940s, beyond which the signal rebounded and increased with time until the 1960s. The interannual variability was the strongest from the 1960s, especially in the late 20th century.

We also analyzed a set of long-term retrospective forecasts of the past 120 years with the HCM. It was found that the model prediction skill displays a consistent interdecadal variation with that of HCA variability, namely that the prediction skill was high in the late 19th century from 1881–1900, and then declined with time, reaching a minimum around 1940–1950s, beyond which it rebounded and increased with time until the 1960s. It had relatively high prediction skill from the 1960s, especially in the late 20th century from 1981–2000. A good relationship between ENSO predictability and the lagged correlation of Niño4 HCA-Niño3 SSTA was also found. These indicate that the interdecadal variation in predictability is highly related to the interdecadal variation of HCA variability itself. A strong HCA signal in the equatorial western Pacific produced a large lagged correlation of Niño4 HCA-Niño3 SSTA, leading to more precursory information at the initial time of predictions. As such, the prediction is likely to be more reliable.

Several cautions should be borne in mind when using the long term HC analysis. First, the oceanic analysis was obtained through forcing the reconstructed wind and historic SST data where the former was

constructed by the line statistical method. The SST data is coarse and gappy before 1950s, thus it might only contain useful information on large-scale interannual or decadal/interdecadal climate variability. Such information might be sufficient to describe and characterize some large-scale climate modes such as ENSO, but not enough for relatively short and small scale variability such as some tropical oceanic waves. Thus the HC analysis should be mainly used for studying large-scale climate signals. Second, the long-term trend was removed from SST prior to constructing the wind in order to manifest the signal of the interannual variability, thereby precluding the long-term trend in the HC analysis. This suggests that the HC analysis might not be suitable for studying the issues related to the global warming that has been detected in the upper ocean (e.g. White *et al.*, 2003). Third we used a running window of 20-yr to analyze interdecadal variations in predictability and the HC variability. The window length of 20 years was motivated by Chen *et al.* (2004) where the interdecadal variations in predictability were discussed in such interval. We also performed several sensitivity experiments, with the window length of 10-yr, 30-yr and 40-yr. The relationships of predictability to the HCA signal are similar to those presented in this paper. Finally the reconstructed winds, subject to a common statistical problem, generally underestimate the amplitude of wind anomaly, thus underestimating the amplitude of HCA. Nevertheless, this study is to date the first work to produce the tropical Pacific upper ocean heat content analysis for the past 120 years. The HC analysis has led to some interesting findings about ENSO variability and predictability as presented in this paper. It has been posted on the internet and is freely loadable (http://web.unbc.ca/ytang/wind.html). Therefore, this work has both theoretical contribution and practical significance in studying the tropical Pacific climate variability, especially for ENSO.

Acknowledgment

This work is supported by BC — China Innovation and Commercialization Strategic Development Program.

References

1. D. S. Battisti, Dynamics and thermodynamics of a warming event in a coupled tropical atmosphere-ocean model, *J. Atmos. Sci.* **45** (1988) 2889–2919.
2. D. W. Behringer, M. Ji and A. Leetmaa, An improved coupled model for ENSO prediction and implications for ocean initialization. Part I: The ocean data assimilation system, *Mon. Weather Rev.* **126** (1998) 1013–1021.

3. D. Chen, M. A. Cane, A. Kaplan, S. E. Zebiak and D. Huang, Predictability of El Nino in the past 148 years, *Nature*, vol. 428, pp. 733–736.
4. Z. Deng, Y. Tang and X. Zhou, The retrospective prediction of ENSO from 1881–2000 by a hybrid coupled model (I): SST assimilation with Ensemble Kalman Filter, *Climate Dyn.* (2008), doi 10.1007/s00382-008-0399-1.
5. Z. Deng and Y. Tang, The retrospective prediction of ENSO from 1881–2000 by a hybrid coupled model (II): Interdecadal and decadal variations in predictability, *Climate Dyn.* (2008), doi 10.1007/s00382-008-0398-2.
6. G. Evensen, The ensemble Kalman filter: Theoretical formulation and practical implementation, *Ocean Dyn.* **53** (2003) 343–367.
7. F. F. Jin, An equatorial recharge paradigm for ENSO. Part I: Conceptual model, *J. Atmos. Sci.* **54** (1997) 811–829.
8. E. Kalnay *et al.*, The NCEP/NCAR 40-year reanalysis project, *Bull. Am. Meteor. Soc.* **77** (1996) 437–470.
9. W. S. Kessler, Is ENSO a cycle or a series of events? *Geophys. Res. Lett.* **29** (2002) 2125, doi:10.1029/2002GL015924.
10. M. Latif, D. Anderson, T. Barnett, M. Cane, R. Kleeman, A Leetmaa, J. O'Brien, A Rosati and E. Schneider, A review of the predictability and prediction of ENSO, *J. Geophys. Res.* **103** (1998) 14375–14393.
11. M. Latif and N. E. Graham, How much predictive skills is contained in the thermal structure of an Oceanic GCM? *J. Phys. Oceanogr.* **22** (1992) 951–962.
12. S. Levitus and T. Boyer, NOAA/OAR/ESRL PSD, Boulder, Colorado, USA (1998), http://www.cdc.noaa.gov.
13. K. Lohmann and M. Latif, Tropical Pacific decadal variability and the subtropical-tropical cells, *J. Climate* **18** (2005) 5163–5178.
14. J.-J. Luo, S. Masson, S. Behera, S. Shingu and T. Yamagata, Seasonal climate predictability in a coupled OAGCM using a different approach for ensemble forecasts, *J. Climate* **18** (2005) 4474–4495.
15. G. Madec, P. Delecluse, M. Imbard and C. Levy, OPA 8.1 Ocean General circulation model reference manual, Institut Pierre Simon Laplace (IPSL) (1998), p. 91.
16. M. J. McPhaden, Tropical pacific ocean heat content variations and ENSO persistence barriers, *Geophys. Res. Lett.* **30** (2003) 1480, doi:10.1029/2003GL016872.
17. C. S. Meinen and M. J. McPhaden, Observations of warm water volume changes in the equatorial Pacific and their relationship to El Niño and La Niña, *J. Climate* **13** (2000) 3551–3559.
18. A. H. Monahan and A. Dai, The spatial and temporal structure of ENSO nonlinearity, *J. Climate* **17** (2004) 3026–3036.
19. A, J. Moore, Y. Zavala-Garay, R. Tang, J. Kleeman, A. Vialard, K. Weaver, D. L. Sahami, T. Anderson and M. Fisher, Optimal forcing patterns for coupled models of ENSO, *J. Climate* **19** (2006) 4683–4699.
20. T. Nakaegawa, M. Kanamttsu and T. M. Smith, Interdecadal trend of prediction skill in an ensemble AMIP-type experiment, *J. Climate* **15** (2004) 2881–2889.
21. J. D. Neelin, D. S. Battisti, A. C. Hirst, F.-F. Jin, Y. Wakata, T. Yamagata and S. Zebiak, ENSO theory, *J. Geophys. Res.* **103** (1998) 14261–14287.

22. M. Rajeevan and M. J. McPhaden, Tropical pacific upper ocean heat content variations and Indian summer monsoon rainfall, *Geophys. Res. Lett.* **31** (2004) L18203, doi:10.1029/2004GL020631.
23. T. M. Smith and R. W. Reynolds, Improved extended reconstruction of SST (1854–1997), *J. Climate* **17** (2004) 2466–2477.
24. M. J. Suarez and P. S. Schopf, A delayed action oscillator for ENSO, *J. Atmos. Sci.* **45** (1988) 3283–3287.
25. Y. Tang and R. Kleeman, A new strategy for SST assimilation for ENSO prediction, *Geophy. Res. Lett.* (2002), 10.1029/2002GL014860.
26. Y. Tang and W. W. Hsieh, ENSO simulation and predictions using a hybrid coupled model with data assimilation, *J. Japan Meteorol. Soc.* **81** (2003) 1–19.
27. Y. Tang, R. Kleeman and A. Moore, SST assimilation experiments in a tropical Pacific Ocean model, *J Phys. Oceangr.* **34** (2004) 623–642.
28. Y. Tang, R. Kleeman and A. Moore, On the reliability of ENSO dynamical predictions, *J. Atmos. Sci.* **62** (2005) 1770–1791.
29. Y. Tang, Z. Deng, X. Zhou, Y. Cheng and D. Chen, Interdecadal variation of ENSO predictability in multiple models, *J. Climate* (2008).
30. K. E. Trenberth, J. M. Caron, D. P. Stepaniak and S. Worley, Evolution of El Nino southern oscillation and global atmospheric surface temperatures, *J. Geophys. Res.* **107** (2002) 4065, doi:10.1029/2000D000298.
31. W. B. White, Design of a global observing system for gyre-scale upper ocean temperature variability, *Prog. Oceanogr.* **36** (1995) 169–217.
32. W. B. White, M. D. Dettinger and D. R. Cayan, Sources of global warming in the upper ocean on decadal period scales, *J. Geophys. Res.* **108** (2003) 3248, doi: 10.1029/2002JC001396.
33. K. Wyrtki, Water displacements in the Pacific and the genesis of El Niño cycles, *J. Geophys. Res.* **90** (1985) 7129–7132.
34. Y. Xue, T. M. Smith and R. W. Reynolds, Interdecadal changes of 30-yr SST normals during 1871–2000, *J. Climate* **15** (2003) 1601–1612.
35. J.-Y. Yu and H.-Y. Kao, Decadal changes of ENSO persistence barrier in SST and ocean heat content indices: 1958–2001, *J. Geophys. Res.* **112** (2007) D13106, doi:10.1029/2006JD007654.
36. S. E. Zebiak, Oceanic heat content variability and El Niño cycles, *J. Phys. Oceanogr.* **19** (1989) 475–486.